REAL-TIME IMPLEMENTATION OF A SINGLE-PHASE ASYNCHRONOUS MOTOR DRIVE FEEDING WITHIN AN OPEN ENERGY SOURCE

Essamudin A. EBRAHIM   and   **Emad SWEELM**
Power Electronics and Energy Conversion Department,   Photovoltaic Department,
Electronics Research Institute (ERI)
Joseph Tito Street, Huckstep, Qism El-Nozha, Cairo Governorate, P. O. Pox 16222, Cairo, Egypt
essamudin@eri.sci.eg,   emadsweelem@eri.sci.eg

Abstract: *A modified nanogrid (MnG) is a very small scalable grid with a low power single-input multi-output (SIMO) inverter. This inverter simultaneously produces both AC and DC currents, such as the switched boost inverter (SBI) and the z-source inverter. These inverters are suitable for low-power loads such as home appliances that use fractional horse-power motors as single-phase asynchronous drives. Thus, this article proposes a single-phase induction motor powered from a modified nanogrid that involves multiple types of inverters such as a SBI and a ZS inverter. The modified nanogrid is mainly dependent on photovoltaic (PV) as a renewable resource. Thus, this manuscript involves a full design for this proposed grid with its maximum power point tracking (MPPT) and the mathematical models for motor drive with both a SBI and a ZSI. Time-varying speed trajectories are proposed to test the robustness of the proposed drives relative to the fluctuation of PV-parameters like its irradiance. Test results are obtained using the Matlab/ Simulink software package and a comparison with the traditional sinusoidal pulse width modulation (SPWM) inverter as a single-input single-output inverter (SISOI). The results indicate that the proposed single-input multi-output inverters are suitable for driving these motors through start-up and operation, although the DC-link voltage is minimized. Furthermore, the proposed system is experimentally implemented with OPAL RT-4510v real-time hardware in the loop (HIL), rapid control prototyping, OP-8660 HIL controller and data acquisition platform.*

Key words*: DC-modified nanogrids (DC-MnG), Open Energy Source (OES), Real-time simulator (RTS), Single-phase asynchronous motor (SPAM), Switched Boost Inverter (SBI)*, Z-Source Inverter (ZSI),

1. Introduction

Induction motors are still widely used in most industrial, commercial and electrical household applications. They are robust, cost-effective, maintenance-free, and have a high power-to-weight ratio [1]-[3]. In contrast, single-phase fractional horsepower induction motors are widely used in a variety of household appliances such as refrigerators, washing machines, and water pumping [4]-[7].

There are several types of these motors are classified according to their starting such as: capacitor starting, capacitor-starting capacitor running, split-phase and shaded pole induction motors [8].

In the past and to date, many efforts have been made to improve and enhance the performance of these motors as variable speed drives. These proposed techniques use a field-oriented vector control for speed tracking such as in [9]-[13].

However, these motors can be powered from the main grid or from an open energy source (OES). The open energy source is a combination of a huge number of DC-nano-grids (DCnGs) that have connected to one another via a DC-link. They contain renewable resources – such as PV, wind, fuel cells, batteries – which are used to power both the DC and AC loads through converters. The traditional nano-grid involves a two-stage converter. It is known as a single-input single output (SIMO) converter. This type uses many components and requires many circuitry to protect [14]-[15]. On the other hand, the DCMnGs involve single-input multi-output converters that simultaneously produce both the DC and AC currents [16],[17]. However, the DC input voltage to the inverter plays a significant rule on its AC output voltage. If the DC-nanogrid is a standalone/ off-grid connection, its AC-output voltage must be well controlled to ensure the sufficient voltage value needed to control the speed and torque of these motors. Most renewable energy sources such as PVs produce a variable DC-voltage based on their irradiation. This DC-voltage is directly proportional to the input radiation. Therefore, if it is cloudy or dark, the AC output voltage will be reduced. Depending, the performance of the asynchronous motor will be

affected during starting and running. Thus, it should increase the AC-input voltage to maintain the torque and speed with proper values keeping the motor running safe with the load. The SBI and ZSI can do that [18]-[23]. Thus, this article introduces a single-phase induction motor (SPIM) with starting capacitor - powered from an open energy source through a single input multi-output inverter (SIMOI). The voltage/ frequency control technique is offered to maintain the internal torque constant through speed change. A robust DC-link voltage controller is provided to maintain the DC-link voltage of the SBI constant. In addition, z-source inverter will be compared with the SBI and the conventional (SPWM) as a single-input single-output (SISO) inverter. The best will be implemented in real-time with the help of OPAL RT-hardware in the loop (HIL) with rapid control prototyping platform. This real-time emulator will be connected through OPAL OP8660 HIL controller and data acquisition module. The real time results are also obtained with the help of the Matlab/ Simulink program for a gradual speed trajectory with different PV-supplies dependent on their insolation. This manuscript is organized a long the following lines: section 1 is introduction. The proposed system with SIMO inverters and the mathematical model of the motor are elaborated in sec. 2. Section 3, provides an explanation for both SBI and z-source inverter. The proposed master and slave controllers for both speed and maximum power point tracking (MPPT) are detailed in sections 4 and 5 respectively. A comparison with the simulation results for the proposed inverter and other systems is conducted in section 6. Real-time emulation of the developed and selected system is implemented using OPAL- RT in section 7. Finally, Section 8 summarizes the research and its conclusion.

2. The proposed SPAM-drive control system

The proposed system comprises SPAM with its two windings, the open energy system (OES), and the controller (as shown in Figure 1). In the following sections, each subsystem will be explained in some detail.

2.1. Single phase asynchronous motor model

This machine is equipped with two windings: main and auxiliary. There are four modes of operation as: split-phase, capacitor starting, capacitor-starting capacitor-running, and main and auxiliary winding mode. In this study, a capacitor-starting single-phase induction motor (SPIM) is used.
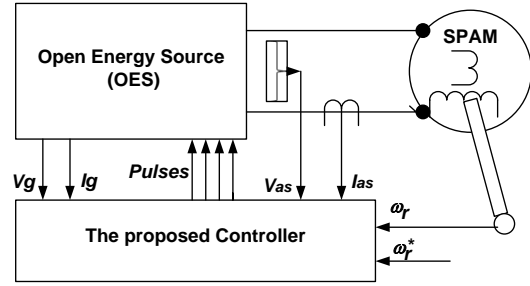

Fig. 1 the proposed SPAM- drive fed from an OES

2.1.1. The mathematical model of SPIM

The dq-reference frame equations for the electrical model for both stator and rotor of SPIM are [24]:

$$V_{sd} = (R_{sd} + pL_{sd}).i_{sd} + pL_{md}.i'_{rd} \qquad (1)$$

$$V_{sq} = (R_{sq} + pL_{sq}).i_{sq} + pL_{mq}.i'_{rq} \qquad (2)$$

$$0 = (p.L_{md}).i_{sd} - (\frac{N_d}{N_q}.\omega_r.L_{mq}).i_{sq} + (R'_{rd} + pL'_{rd}).i'_{rd} - (\frac{N_d}{N_q}.\omega_r.L'_{rq}).i'_{rq} \qquad (3)$$

$$0 = (p.L_{mq}).i_{sq} - (\frac{N_q}{N_d}.\omega_r.L_{md}).i_{sd} + (R'_{rq} + pL'_{rq}).i'_{rq} - (\frac{N_q}{N_d}.\omega_r.L'_{rd}).i'_{rd} \qquad (4)$$

Where,
$$L_{sd} = L_{lsd} + L_{md} \qquad (5)$$
$$L_{sq} = L_{lsq} + L_{mq} \qquad (6)$$
$$L'_{rd} = L'_{lrd} + L'_{md} \qquad (7)$$
$$L'_{rq} = L'_{lrq} + L'_{mq} \qquad (8)$$

The instantaneous electro-magnetic internal torque of the motor can be computed as:

$$T_e = \frac{P}{2}.\frac{N_d}{N_q}.L_{mq}.(i_{sq}.i'_{rd} - i_{sd}.i'_{rq}) \qquad (9)$$

The dynamic equation is:

$$p.\omega_r = \frac{1}{J_m}.(T_e - T_l) \qquad (10)$$

Where, V_{sd}, V_{sq} are the stator voltage in dq-axis frame, R_{sd}, R_{sq} are the stator resistance in dq-axis frame. L_{sd}, L_{sq} are the stator inductance in dq-reference frame, p is the differential operator (*d/dt*), i_{ds}, i_{qs} are the stator currents in dq-frame, L_{md}, L_{mq} are the mutual inductances in dq-frame, N_d, N_q are the effective turns in dq-frame, R'_{rd}, R'_{rq} are the rotor resistance referred to stator in dq-frame, i'_{rd}, i'_{rq} are the rotor current referred to stator in dq-frame, L'_{rd}, L'_{rq} are the rotor inductance referred to stator in dq-frame, ω_r is the rotor angular speed, L'_{lrd}, L'_{lrq} are the leakage inductance of rotor in dq-frame, L_{lsd}, L_{lsq} are the leakage inductance of stator in dq-frame, T_e is the motor electrical internal torque, P is the number of pair pole of the motor, and J_m is the motor inertia.

In the above equations, the auxiliary winding represents d-axis components and the main winding represents the q-axis components. So, the supply voltage V_{supply} equal to V_{sq} as:

$$V_{supply} = V_{sq} \tag{11}$$

$$V_{sd} = V_{supply} - \frac{1}{C} \int i_{sd} dt \tag{12}$$

Where, C is the capacitor connected for starting.

2.2. An Open Energy Source (OES)

OES consists of several huge nanogrids that are connected to each other through a DC-link. These interconnected nanogrids are controlled with a smart system to manage the flow of power to each other. Each nanogrid has a power converter to produce both DC and AC supplies. The classical nanogrid uses a two-stage converter-inverter set. But, the modified nano-grid contains a SIMO-inverter. There are two types of SIMO-inverters: switched boost inverter (SBI) and z-source inverter (ZSI). For this study, the PV is selected as a renewable source used to power all grids. An array of PV is arranged as number of series N_s and parallel N_p modules are connected with each other to provide the required power with the appropriate terminal voltage. In this case, the SunPower SPR 305WHT (appendix A) module is used. Also, we selected 2 in series and 10 in parallel to supply about 6 KW.

3. Single input multi-output inverter (SIMOI)

Through the following lines, both the SBI and ZSI with some detail will be explained. Furthermore, a comparison between SIMOI and SISOI (such as the sinusoidal PWM inverter) will performed. Thus, SISOI will also be brief explained.

3.1. Switched boost inverter (SBI)

As shown in Figure 2, SBI consists of five IGBTs, 2-diodes, one coil, and one capacitor to transmit the power from the PV-source to the motor. It depends on two modes of operation: the shoot-through and non-shoot through techniques to turn-on and off switches. This technique protects all switches from short-circuit current and there is no need to dead-time delay circuit to avoid overlapping between two IGBTs on the same inverter leg. Its output can be controlled directly to upward or downward the DC and /or AC voltage values. Thus, when it is supplied from the PV-intermittent source, it increases its AC-output voltage to sufficient value that produces the torque required to start-up the motor with a pre-scribed speed.

In the non-shoot through state, $t_{off} = (1-D) \times T_s$, the switch S is turned off and the inverter bridge is represented by a current source. Where, t_{off} is the turn off time for the switch S, D is the duty ratio, and T_s is the periodic time for switch S equal ($t_{off} + t_{on}$) and t_{on} is the turn-on time. Now, the voltage of the renewable source (i.e., PV)(V_g), and the energy stored in the inductor L together will supply the inverter and the capacitor through diodes D_a and D_b.

The inductor current in this interval equals the capacitor charging current added to the inverter input current. Note that the inductor current is assumed to be sufficiently high for the continuous conduction of diodes D_a and D_b for the entire interval. The inductor current (I_L) will exceed linearly to a value equal to that of the capacitor charging current added to the DC load current and the inverter input current (assuming continuous conduction mode) for the interval $((1-D) \times T_s)$. The SBI utilizes the shoot-through interval of the H-bridge to appeal to the boost operation. So, the traditional PWM control technique of the traditional voltage source inverter (VSI) should be modified to incorporate the shoot-through state to be suitable for the SBI [25].

The PWM scheme for SBI is developed based on the traditional sine-triangle PWM with voltage switching level. This technique has been illustrated during positive and negative half cycles of the sinusoidal modulation signal $v_m(t)$ and is given in details in [26]-[28]. However, the DC-output voltage of SBI can be computed as:

$$\frac{V_{DC}}{V_g} = \frac{1-D}{1-2D} \tag{12}$$

Where, V_{DC} is the DC-link voltage of the inverter. It should be noted that the shoot-through state of the inverter bridge will not affect the harmonic spectrum of the inverter's output voltage if the sum of shoot-through duty ratio (D) and the modulation index (M) is less than or equal to unity.

$$M + D \leq 1 \tag{13}$$

Hence, the values of M and D are chosen according to the peak value of the AC output voltage $\tilde{V}_{AC}$ that is given by:

$$\tilde{V}_{AC} = M.V_{DC} = M.\frac{1-D}{1-2D}.V_g \tag{14}$$

3.2. Z-Source inverter

As shown in Figure 3, it contains more passive elements than SBI. It implies two identical coils and capacitors – for symmetrical one – to prevent short-circuit current when the switches are conducting and 4- IGBTs as a classical inverter and one diode to block reverse current. There are three modes of
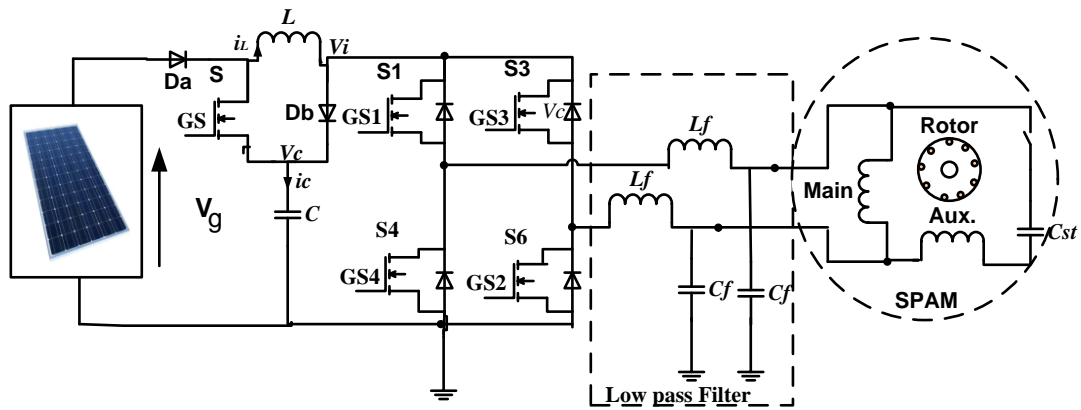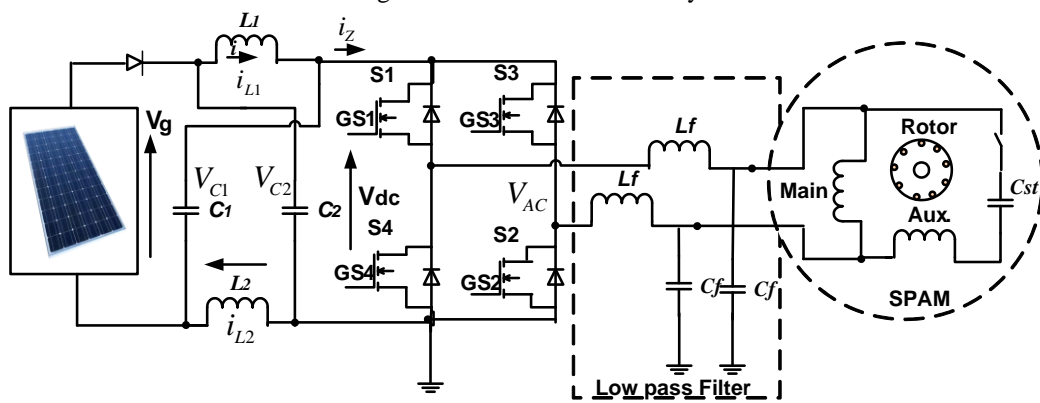
Fig. 2 SPAM fed from PV-array via a SBI

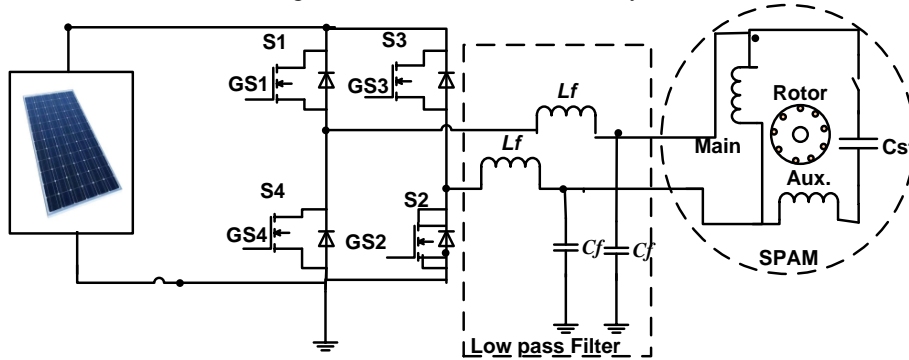Fig. 3   SPAM fed from PV-array via a ZSI

Fig. 4   SPAM fed from PV-array via a SISO inverter

Table 1. Switching modes of z-source inverter operation

Switching States (Modes)	S_1	S_4	S_3	S_2	Output voltage
Active state	1	0	0	1	Finite Voltage
	0	1	1	0	
Zero state	1	0	1	0	Zero
	0	1	0	1	
Shoot-through state	1	1	S_3	S_2	Zero
	S_1	S_4	1	1	
	1	1	1	1	

operation for z-source inverter: the active state, zero state, shoot-through zero state. Table 1 describes these operating states.

The voltage across each capacitor is equal and the current through each coil is also equal. So, in shoot-through state, $V_Z = 0$, if the duty ratio D_Z is equal to (T_S/T), where T_s is the total shoot-through time through one cycle and T is the periodic time, then, applying Kirchhoff's Lows:

$$\begin{cases} v_{L1} = v_{C1} = v_{L2} = v_{C2} \\ i_{C1} + i_{L1} = i_{C2} + i_{L2} = 0 \\ i_Z = i_{L1} - i_{C2} = i_{L2} - i_{C1} \end{cases} \tag{15}$$

$$\begin{aligned} v_{L1} = v_{L2} &= V_g - v_{C1} = V_g - v_{C2} \\ V_{dc} &= 2. v_{C1} - V_g \\ i_{L1} &= i_{C2} + i_Z \\ i_{L2} &= i_{C1} + i_Z \end{aligned} \tag{16}$$

$$\frac{d}{dt}\begin{bmatrix} i_{L1}(t) \\ i_{L2}(t) \\ v_{C1}(t) \\ v_{C2}(t) \end{bmatrix} =$$

$$\begin{bmatrix} 0 & 0 & \frac{(2.D_Z-1)}{L_Z} & 0 \\ 0 & 0 & 0 & \frac{(2.D_Z-1)}{L_Z} \\ \frac{-D_Z}{C_Z} & \frac{1-D_Z}{C_Z} & 0 & 0 \\ \frac{1-D_Z}{C_Z} & \frac{-D_Z}{C_Z} & 0 & 0 \end{bmatrix} \cdot \begin{bmatrix} i_{L1}(t) \\ i_{L2}(t) \\ V_{C1}(t) \\ V_{C2}(t) \end{bmatrix} +$$

$$\begin{bmatrix} \frac{1-D_Z}{L_Z} \\ \frac{1-D_Z}{L_Z} \\ 0 \\ 0 \end{bmatrix} \cdot V_g + \begin{bmatrix} \frac{D_Z-1}{C_Z} \\ \frac{D_Z-1}{C_Z} \end{bmatrix} \cdot i_Z \tag{17}$$

The steady state parameters can be obtained by setting equation (17) to zero:

The state-space equation for the Z-inverter can be written as follows:

$$v_{C1} = v_{C2} = \frac{1-D_Z}{1-2.D_Z}. V_g = V_{dc}$$

$$V_{dcp} = \frac{1}{1-2.D_Z}. V_g \tag{18}$$

$$i_{L1} = i_{L2} = \frac{1-D_Z}{1-2.D_Z}. i_Z$$

According to the equation (18), the AC- peak output voltage of the inverter can be determined as:

$$\hat{V}_{AC} = \frac{\hat{V}_m}{\hat{V}_{Car}}. \bar{V}_{dc} = m_a. \left(\frac{D_Z-1}{2.D_Z-1}\right). \bar{V}_{dc} \tag{19}$$

Where, $\hat{V}_m$ is the peak value of the modulation wave (i.e., sine wave), $\hat{V}_{Car}$ is the peak value of the carrier wave (i.e., triangular wave), m_a is the modulation

index of the inverter, $\bar{V}_{dc}$ is the dc-link voltage of the inverter. For more details about two-level z-source inverter, it can be referred to [29]-[32].

3.3. THE SINUSOIDAL PWM-SISOI

The sinusoidal-PWM inverter is considered as a single-input single-output inverter which has only one DC-input voltage and only one AC-output voltage. It can be supplied directly from the DC-source such as PV or battery bank as shown in Figure 4.

4. THE MASTER SPEED CONTROL AND MPPT ALGORITHM

The block diagram for the master speed controller is shown in figure 5. The controller strategy depends on the variation of both voltage and frequency with the same rate – as a scalar value – to keep the motor internal torque constant. The reference frequency and voltage can be computed according to the following equations:

$$f_r = \frac{PN_r}{60} \tag{20}$$

$$e(t) = (f_r^* - f_r) \tag{21}$$

Where P is the number of pair-poles, f_r^*, f_r is the rotor reference and actual frequency and e is the error signal. The output of the PI-controller is the slip-frequency f_{slip}:

$$f_{slip} = K_p. e(t) + K_i \int e(t)dt = K_p. (f_r^* - f_r) + K_i \int (f_r^* - f_r)dt \tag{22}$$

Then, the reference synchronous frequency f_s^* of the motor can be computed as:

$$f_s^* = f_r + f_{slip} \tag{23}$$

The reference voltage peak- value V_m^* :

$$V_m^* = K_{vf}. f_s^* \tag{24}$$

Where, K_{vf} is a constant depends on flux and selected according to the rated frequency and voltage of the machine. For this work, this value is equal 2.4 for the test machine.

The main purpose of this control is to generate the modulation signal required to produce IGBTs gating signals for all inverters. So, the sinusoidal signal can be computed – according to the block diagram of Fig. 6-a as:

$$v_m(t) = V_m^*. Sin\, \theta_r^* \tag{25}$$

Where, θ_r^* is the reference position angle and can be computed from the reference frequency as:

$$\theta_r^* = \int \omega_r^*. dt = \int 2. \pi. f_r^*. dt \tag{26}$$

This modulated signal is compared with the triangle signal according the modulation index M as:
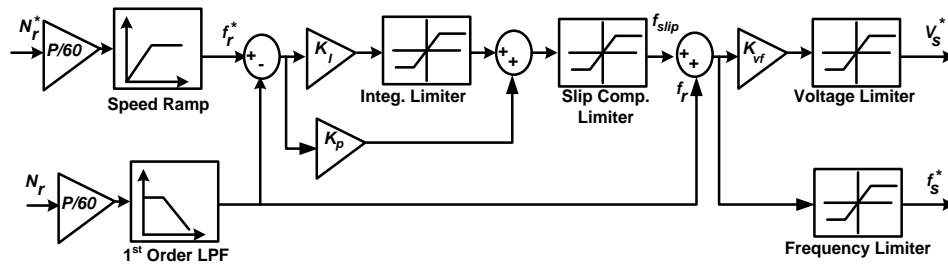
$$M = \frac{V_m^*}{V_P^*} \tag{27}$$

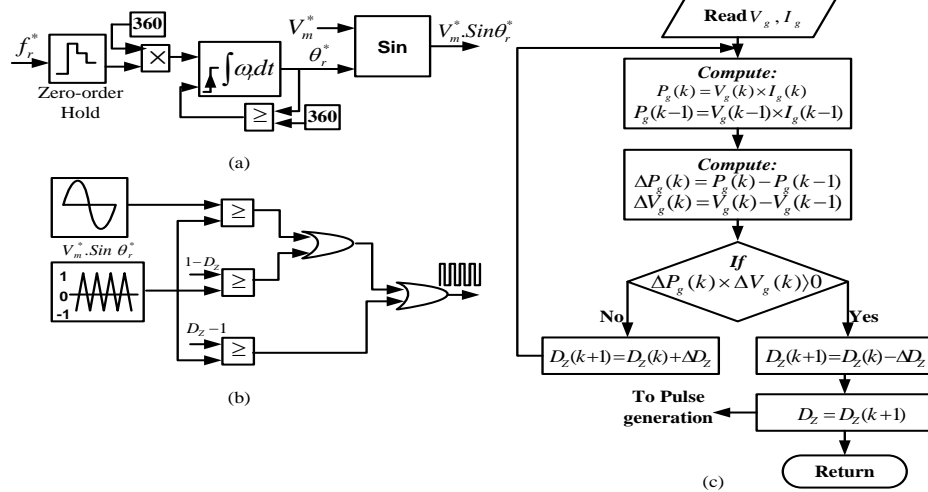Fig.5 The master controller (sequence of scalar speed control V/f block diagram)

Fig. 6 Slave control: (a) MPPT flow chart (b) modulator-signal generation
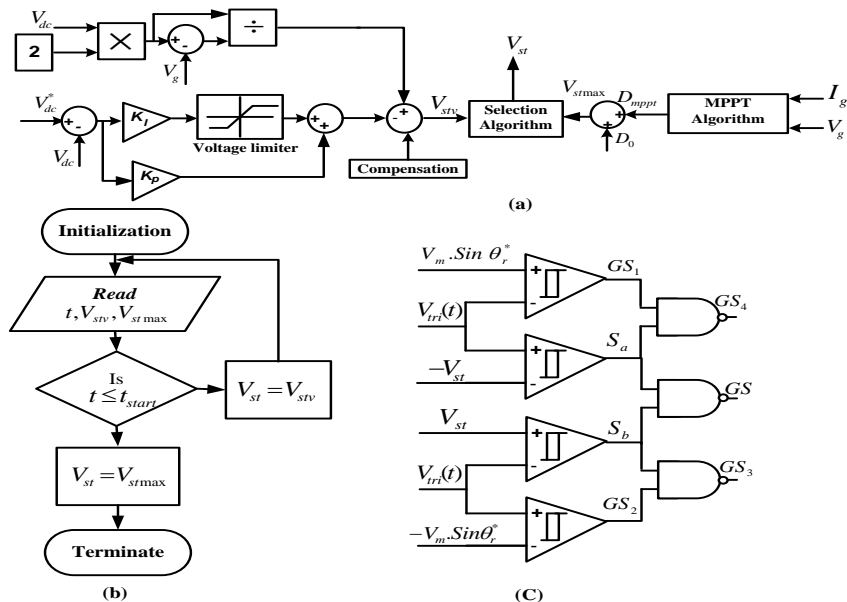(c) modified sine triangle PWM generation

Fig. 7 SBI-Voltage control (a) DC-link voltage control (b) starting algorithm (c) logic gating signals

Table 2 the main parameters for both Z-source and SBI inverters

SBI parameters [16]			ZSI-parameters [33]		
parameter	value	unit	parameter	value	unit
Inductance of main inductor (L)	5	mH	Inductance of main coils ($L_1 = L_2$)	1	mH
Capacitance of main capacitor (C)	1500	μF	Capacitance of main capacitors ($C_1 = C_2$)	1300	μF
Inductance of filter inductor (L_f)	1	mH	Inductance of filter inductor (L_f)	1	mH
Capacitance of filter capacitor (C_f)	150	uF	Capacitance of filter capacitor (C_f)	150	uF

Where, V_P^* is the peak value of the carrier-triangular wave – as shown in Fig. 6-b.This technique is used for speed control for all compared inverters. But, for SIMOIs, another parameter is used with the combination of M to control the voltage of DC-link and this will directly affect the motor speed and torque. This parameter is the duty ratio D, this can be controlled according to the maximum power point tracking (MPPT) for the PV-array. In this research, the hill-climbing algorithm is used as a MPPT. The flow chart for this algorithm is shown in fig. 6-c. The same MPPT algorithm is used for both z-source and SBI inverters. In z-source inverter the duty ration D_z is used in shoot-through period to control the DC-link voltage as shown in Fig. 6-b. But, in the SBI, a proposed DC-link voltage controller is used.

5. DC-LINK VOLTAGE CONTROLLER OF SBI

The block diagram of the DC-link voltage of SBI is depicted in fig. 7-a. This block produces the voltage level control signal (V_{ST}) that is needed for shot-through signals controlling the switch (S).The control algorithm depends on introducing a mathematical model for the actual value of V_{ST} that can be computed as follows [16]:

From the strategy and analysis of the SBI, $+V_{ST} = V_p(1-D)$, $-V_{ST} = -V_p(1-D)$, so:

$$D = 1 - \frac{V_{ST}}{V_P} \tag{28}$$

If $V_P = 2$, by substituting in eqn. 28,

$$D = 1 - \frac{V_{ST}}{2} \tag{29}$$

By substituting in eqn. 12 from 29,

$$V_{ST} = \frac{2*V_{dc}}{2*V_{dc}-V_g} \tag{30}$$

The block diagram for this model is drawn as a reference according to Eqn. 30. Also, its output is added to the output of the PI-controllers used for voltage control loop with compensation - as shown in Figure 7-a. Two operating modes are offered. The first one is proposed through starting to keep the voltage of DC-link constant. This increases the voltage to its maximum value and the second algorithm achieves MPPT as shown in Fig. 6-c. The output control signal of the voltage control is denoted by V_{stv}. On the other hand, the control signal in case of MPPT is denoted by V_{stmax}.The flow chart of this algorithm is shown in Fig. 7-b. This algorithm depends mainly on the starting time t_s. If the time is less than or equal to the motor start-up time, the controller maintains the motor voltage constant through start-up. After this, the operation time increases to more than start-up time, thus activating the MPPT algorithm. The digital logic

gates required to generate the 5-control gating signals for the IGBTs of the SBI is shown in Fig. 7-c. For more details referred to [15],[16].

6. Simulation results and discussion

To test the robustness of the proposed system, a comparison between the SIMO and SISO inverters is performed. Two SIMO inverters are tested (i.e., z-source and SBI). The SISO inverter is the sinusoidal PWM which is compared to the other two types. The same motor-speed controller – proposed in Section 4 is used for all types with the same parameters. The gain parameters for PI-speed controller are: $K_p = 3$, and $K_i = 10$. The name plate date of the fractional-horse power test single-phase induction motor and its main parameters are included in appendix B [8]. The PV-array consists of two modules in series and ten in parallel with irradiance varies from 200 to 1000 w/m² at 25° C. The parameters of PI-controller for DC-link voltage control of SBI is: $K_p = 0.00001$ and $K_i = 0.00005$ with limiting block values ∓2. All parameters are selected according to Ziegler-Nichols Formula. The main parameters for both z-source and SBI inverters are presented in Table 2. The switching frequency for all inverters equal 10 KHz. All systems are implemented using the Matlab/Simulink software package (ver. R2018a) [33]. To test the robustness of the proposed system against the DC-link input variation for all inverters, several cases are investigated. The first case is designed using a constant battery input voltage with a value of 126 V. The second case, when all inverters are supplied from a PV-array with a constant irradiance (1000 w/m²) with a 126V output. The third case, is the study of the effect of irradiation on the motor performance when its value is reduced from 1000 to 200 w/m² by starting the motor. Furthermore, the robustness of the controller is also tested by starting, accelerating, and decelerating of the motor. The speed trajectory is considered initially as a ramp with acceleration to increase the motor speed linearly to 1500 rpm across 1 second of start time. Then, the motor reaches to steady state with a constant speed for another second and after that the motor decelerates to 750 rpm over the period (2 to 2.5 seconds). Finally, the motor reaches a speed of 750 rpm and continues to operate at this speed as a steady-state value. The test machine is a single-phase staring-capacitor induction motor. The starting capacitor is used during start-up until the motor reaches to 80 % of its nominal speed (i.e., 1800 rpm).

6.1. Case 1: The motor is powered by a battery bank through the inverters

In this case, the motor is powered by a battery bank - with a constant value equal to 126V- through the aforementioned three inverters. Fig. 8 illustrates the proposed speed trajectory for motor power across all inverters. As can be seen, they all showed a good response with some overshooting compared to the reference speed trajectory. In addition, it can be noted that the speed trajectory with SBI is under damping with minimum overshooting in comparison with the other two types. Figure 9 demonstrates the total stator currents with all inverters. At 80 % of the synchronous speed (i.e., 1440 rpm) the capacitor is cut off. The waveform of internal electric torque of the motor is illustrated as an instantaneous value given in Fig. 10. At start-up, the motor torque is increased until the motor reaches steady state and then decreases to a nominal value.
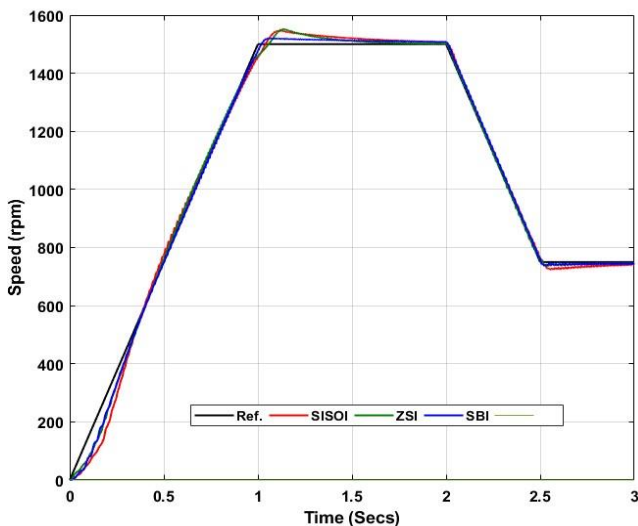
Figure 8 actual and reference forward speed trajectories for inverters with battery bank

6.2. Case 2: The motor is powered by a PV-array without shade

In this case, the motor is delivered by a PV-array through the selected inverters. In this case the PV-irradiance is assumed to be constant without shade and equal to 1000 W/m² - as shown in Figure 11-a.
Figures 11-b and c illustrate the voltage of PV-terminal and the power profiles of this radiation. As stated, at the start the voltage value is roughly constant and equal to 126 V. Then, while starting, its value is affected by switching the load and inverter. It therefore varies slightly according to the motor current and power. The motor speed trajectory is shown in Fig. 12. Due to oscillations in the PV-output voltage, the speed trajectory is also affected accordingly,
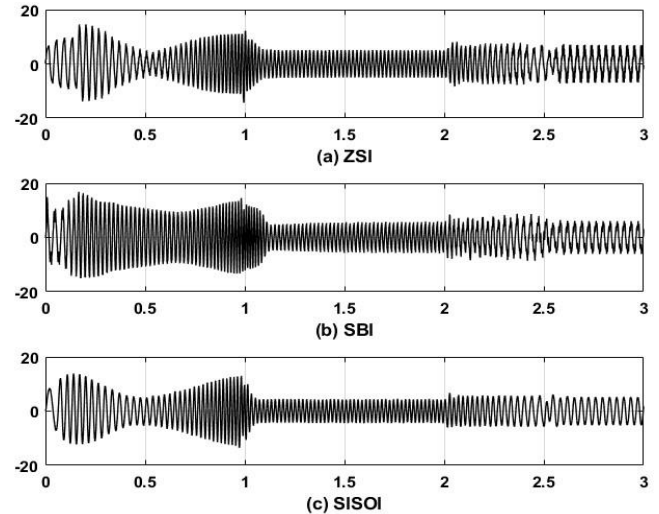

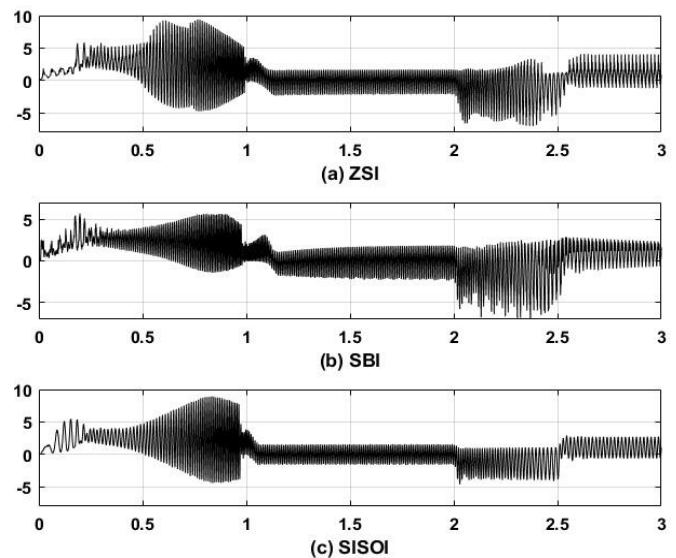Fig. 9 The total stator currents with all inverters

Fig. 10 Motor internal electric torque

especially with the SISO-inverter due to absence of the first stage (i.e., converter). However, both two-stage inverters almost follow the refernce speed trajectory. But, the best drive is that of SBI due to the robust controller offered. In addition, z-source inverter is tracking with a slight deflection. Figure 13 demonstrates the stator total currents. As shown, when starting the current will increase and then decrese in steady state. As shown, when the motor reaches to 80% of the nominal speed, the capcitor circuit is open. It depends on the temporal response of each proposed system based on its controller and the voltage of the DC-link. Likewise, SBI is much faster than others with minimum overshot. Accordingly, the internal electrical torque, shown in Figure 14, is also affected by the DC-link input voltage of the inverter.
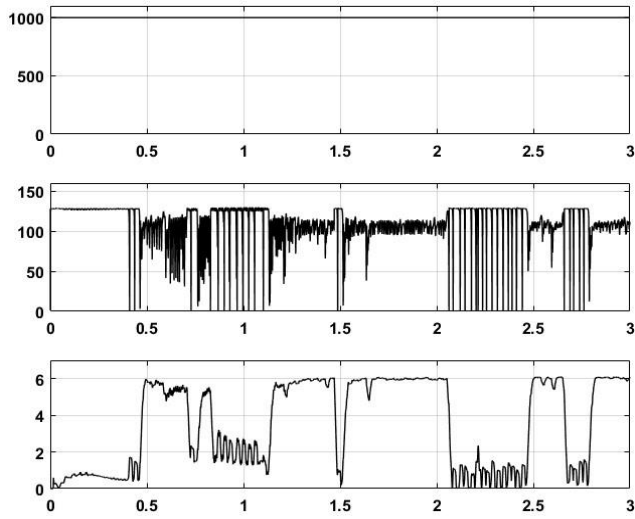
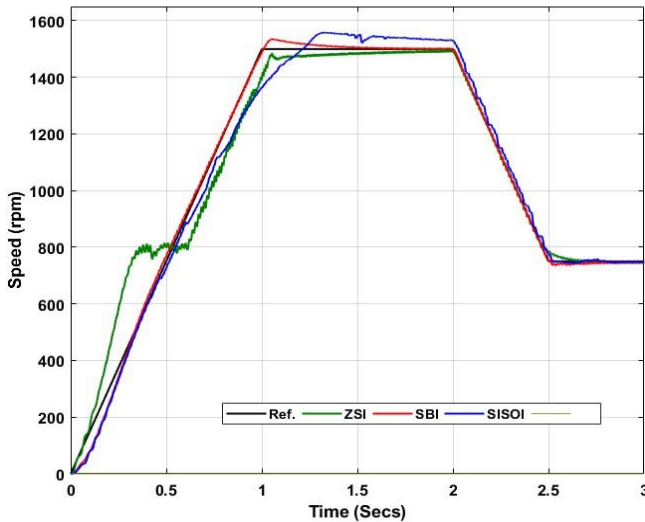Fig. 11 PV-array (a) irradiance (b) voltage (c) power

Figure 12 actual and reference forward speed trajectories for inverters without PV-shadow

Fig. 13 The total stator currents for all inverters

Fig. 14 Motor internal electrical torque

The motor torque gradually increases at start-up and then decreases with the current steady state. As shown, the SISO inverter provides low-starting torque comapred to other two inverter types.

6.3. Case (3): The motor is powered by a PV-array with shade

In this case, the shadow for the PV-array shall be considered. At t-0.5 to 0.6, the insolation is reduced from 1000 W/m² to 200 W/m² during this period as shown in Fig. 15a. Accordingly, the terminal voltage and generated power are shown in Figures 15-b and c. The reference and actual speed trajectories of all compared inverter systems are shown in the Fig. 16. As illustrated, the SBI with the help of the proposed voltage controller and its strategy, succeeded to follow the trajectory through start-up. Although the
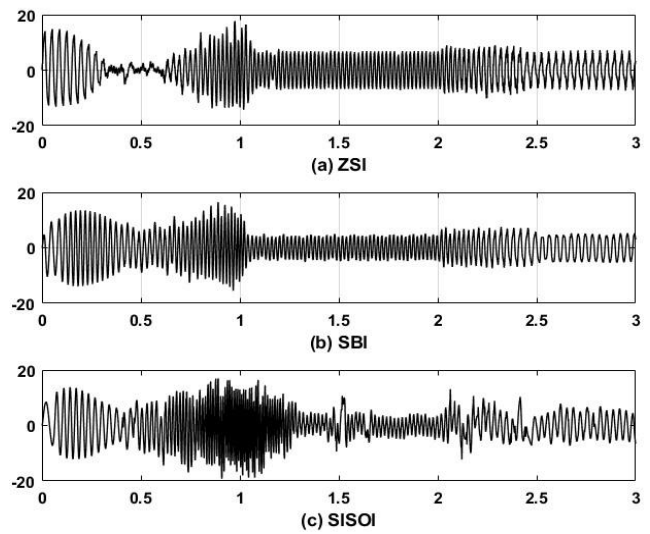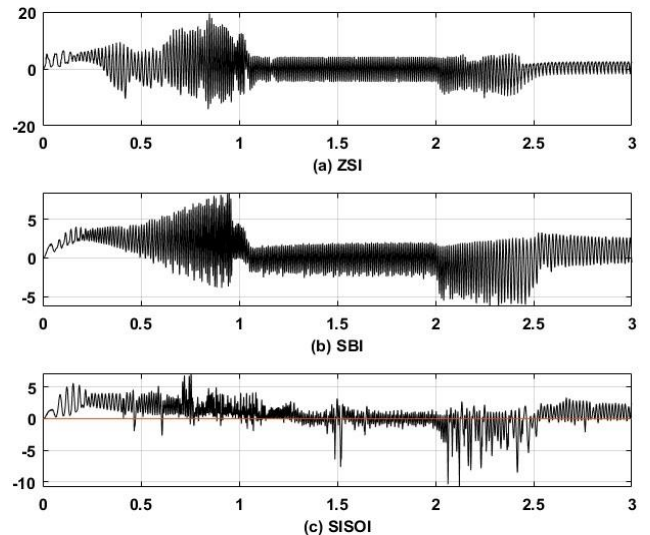
insolation was reduced to its minimum value, the DC-link voltage is increased to a sufficient value.

Moreover, the z-source inverter also followed the trajectory with a time delay and a maximum overshot at startup. The SBI and z-source inverters followed the speed trajectory through the deceleration without error. However, the SISO-inverter system took more delay time without deviation of the speed trajectory through starting period. Furthermore, it could not follow the deceleration of speed trajectory. Figure 17 illustrates the stator current. At starting, the motor with both SBI and z-source inverters consumes fewer power than the SISO inverter. This can be illustrated clearly through the internal electrical torque of the motor as shown in Fig. 18. The motor exerted more torque for the SBI and z-source inverters but SISO-inverter produces a bit of torque due to the lake of input DC-voltage.
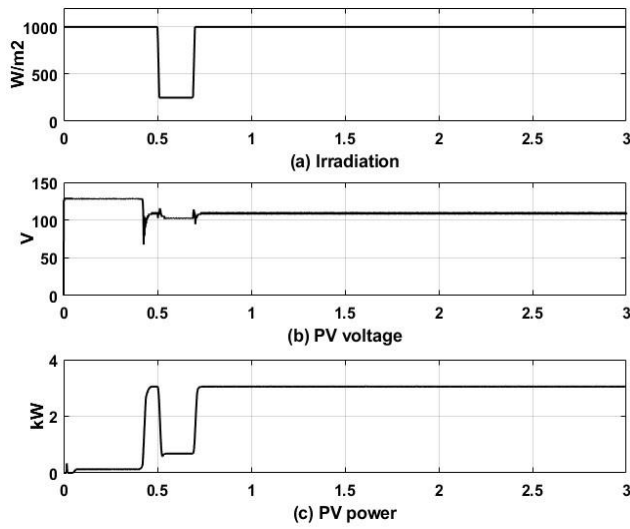
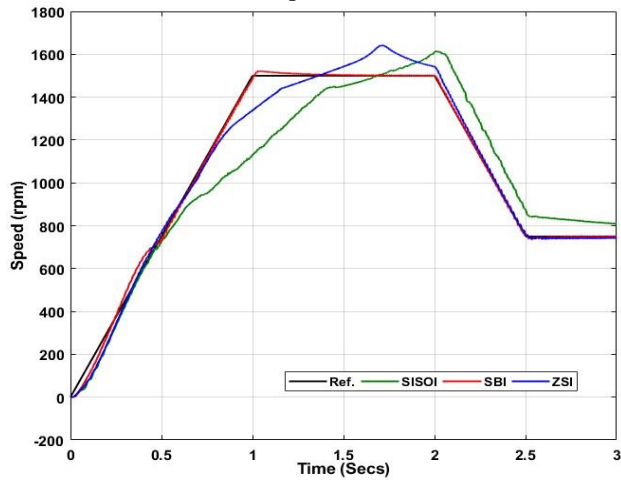Fig. 15 PV- (a) irradiance (b) terminal voltage   (c) output power

Fig. 16 actual and reference forward speed trajectories for inverters with PV-shadow

Fig. 17 The total stator currents for all inverters

Fig. 18 Motor electric internal torques with all inverters

7. Real-time implementation for the SIMO-inverter systems

In power systems and drives, real time simulator (RTS) is used to design, test control, and protect equipment performance before installation on actual state. So, in this work, the combination of OP4510 real-time hardware-in the loop (HIL) and rapid-control prototype (RCP) [34] and OP8660 HIL-controller and data acquisition interface [35] platforms are used to implement the proposed drive.

According to simulation results, the SPIM-drive based on SBI will be only implemented to overcome the parameter variations of the PV-fluctuations. The overall practical system is shown in figure 19. All output parameters of the drive such as speed, torque, capacitor voltage, and currents are measured as real signals through the analog port of the HIL and its
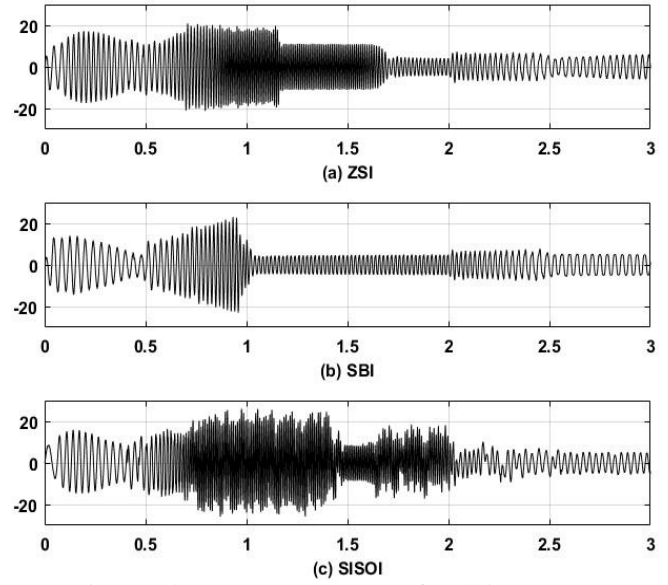
controller. The speed trajectory is scaled down through the Simulink platform by 1000. So, as shown in fig. 20-Chs. B and C, the actual and reference speed trajectories are nearly identical with real scale 1000 rpm/ div. In addition, the electrical internal torque is scaled down by 20 and channel scale is 500mv/div, so as shown in fig. 20-Ch. A, the real-scale value is 5 N.m. /div. The total stator current, main, and auxiliary winding currents are also the real scale is 10 A/div. As illustrated in fig. 21 Chs. A, B, and C, at starting the motor currents are increased and then decreased after steady-state. This can be clearly depicted as shown in fig. 21. The starting capacitor voltage ensures the starting process as illustrated through Ch. D with real-scale 200V/div.
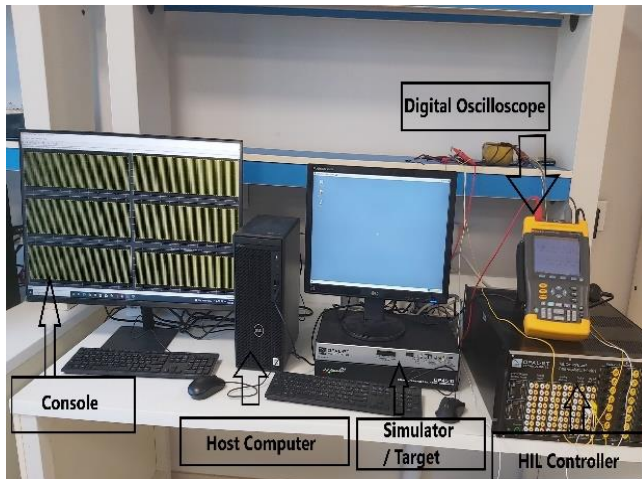
Fig. 19 Experimental rig

Fig. 20 Ch. A: internal torque, Ch. B and C reference and actual speed

8. Conclusion

This article has examined the performance and behavior of a single phase induction motor when fed from an intermittent voltage source, such as a solar cell via SIMO- SBI and z-inverters. This manuscript suggested a scalar voltage/frequency as the master controller for the motor speed. In addition, another slave controller was proposed for DC-link voltage control and MPPT algorithm. This controller contributed to keep the DC-link voltage of the SBI constant to a certain value when the PV-array has a low radiation due to shade or cloudy weather. This value is sufficient to ensure the torque and current of the motor leads to better performance during starting and running. SIMO inverters are the best solution to ensure the best performance for SPIM drives with these intermittent sources compared to the SISO inverters. The proposed system was implemented in a real time. Thus, in the near future, it can be easily deployed as a true physical prototype.

Fig. 21 Ch. A: total stator current, Ch. B main winding, Ch. C: Auxiliary winding currents, and Ch. D capacitor voltage (starting moment)

APPENDIX A
PV-Module Specifications
$P_{STC} = 305W$, $P_{PTC} = 208.6W$, P (I_{max}) = 5.58A, V (P_{max}) = 54.7V, I_{SC} = 5.96A, V_{OC}=64.2V, N_{cell}=96, V_{max}=600V.

APPENDIX B
The motor data: $P_{rated} = 0.25\,HP$, $P = 4$, $V_{rated} = 110\,V$, f_{rated}=60 Hz, $R_{sm} = 2.02\,\Omega$, $X_{lsm} = 2.79\,\Omega$, $X_M = 66.8\,\Omega$, $R_{sa} = 7.14\,\Omega$, $X_{lsa} = 3.22\,\Omega$, $R_{cap.}$= 2.15 Ω, $C_{st.} = 255\,\mu F$, $R'_{lr} = 4.12\Omega$, $X'_{lr} = 2.12\,\Omega$

REFERENCES

[1] E. A. Ebrahim,: *A novel approach of adaptive neuro-PI vector controller fed IM servo drives*, 2002 IEEE/RSJ Int. Conf. , Switzerland, October 2002, pp. 2181-2186.
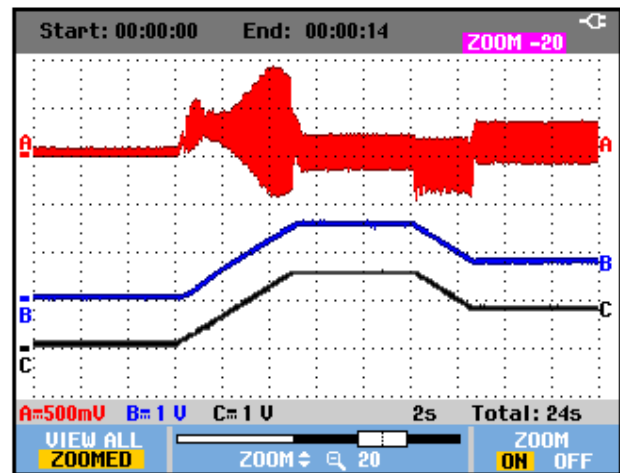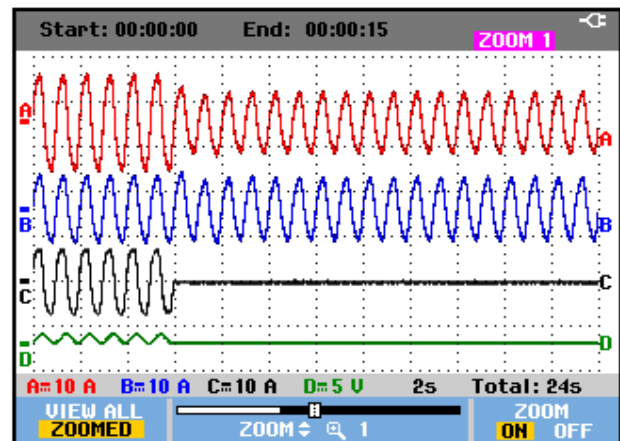
[2] E. A. Ebrahim and N. Hammad,: *Fault analysis of current-controlled PWM-inverter fed induction motor drives*, 7th Int. Conf. on Properties and Applications of Dielectric Materials, Japan, 2003, pp. 1065-1070.

[3] E. A. Ebrahim and A. A. Metwaly,: *Performance and tracking control of three-phase induction-motor drive fed from a DC-modified nano-grid*, WSEAS Transaction on Power Systems, Vol. 16, pp. 8-22, 2021.

[4] N. Ahmed et. al.: *AC chopper voltage controller-fed single-phase induction motor employing symmetrical PWM control technique*, Electric Power Systems Research, Vol. 55, pp. 15–25, 2000.

[5] E. Ribisi and P. Freere,: *Reduced starting current for single phase capacitor induction motors while maintaining starting torque*, 2019 IEEE AFRICON, Ghana, Sep. 2019.

[6] M. Almani et. al.: *An improved technique for energy-efficient starting and operating control of single phase induction motors*, IEEE Access, Vol. 9, pp. 12446-12462, 2021.

[7] S. Wang, J. Kang, and J. Noh,: *Topology optimization of a single-phase induction motor for rotary compressor*, IEEE Transactions on Magnetics, Vol. 40, No. 3, pp. 1591-1596, MAY 2004.

[8] I. Poldea and S. Nasar,: *The induction machines design hand book*, CRC Press, 2010.

[9] M. Corrêa et. al.: *Rotor-flux-oriented control of a single-phase induction motor drive*, IEEE Transactions on Industrial Electronics, Vol. 47, No. 4, pp. 832-841, 2000.

[10] F. Gbaden, et. al.: *Design and implementation of speed adjustment for single phase induction motor*, IOSR Journal of Electrical and Electronics Engineering , Volume 16, Issue 2, PP 09-17, 2021.

[11] A. Nied et. al.: *Single-phase induction motor indirect field oriented control under nominal load*, PEDS2009, Taiwan, pp. 789-793, 2-5 Nov. 2009.

[12] P. Kumbhar, S. *Lokhande,: Embedded based compact fuzzy system to speed control of single phase induction motor*, IOSR Journal of Electrical and Electronics Engineering, Volume 9, Issue 5,PP 56-59, 2014.

[13] V. Vodovozov, N. Lillo, Z. Raud,: *Variable-speed single-phase induction motor drive for vehicular applications*, Electrical Engineering Research, Volume 2, pp. 18-24, 2014.

[14] E. A. Ebrahim, et. al.,: *DC-Based interconnected-modified nano-grids with an open energy distributed system*, (CIRED'19), Madrid, pp. 1-5, 3-6 June 2019.

[15] E. A. Ebrahim, et. al.,: *Photovoltaic Based Interconnected Modified DC Nanogrids within an open energy distribution system*, (ACCS) & (PEIT) IEEE Egypt Section, Cairo, pp. 253-258, 2019.

[16] E. A. Ebrahim, et. al.,: *Closed-loop control of a single-stage switched-boost inverter in modified DC-interconnected nano-grids*, IET, the Journal of Engineering, Vol. 2020, Iss. 10, pp. 843-853, 2020.

[17] E. A. Ebrahim, et. al.,: *Open energy distribution system-based on photo-voltaic with interconnected-modified DC-nanogrids*, (ASTESJ) Journal, Vol. 6, No. 1, pp. 982-988, 2021.

[18] A. Rajaei, et. al.: *Single-phase induction motor drive system using z-source inverter*, IET Electric Power Applications, Vol. 4, Iss. 1, pp. 17– 25, 2010.

[19] S. Rahman et. al.: *Design and implementation of cascaded multilevel qZSI powered single phase induction motor for isolated grid water pump application*, IEEE Transactions on Industry Applications, Vol. 56, Issue 2, pp. 1907-1917, 2020.

[20] B. Ge, et. al.,: *Novel energy stored single-stage photovoltaic power system with constant DC-link peak voltage*, IEEE Transactions on Sustainable Energy, vol. 5, no. 1, pp. 28-36, Jan. 2014.

[21] D. Sun, B. et. al.: *An energy stored quasi-Z-Source cascade multilevel inverter-based photovoltaic power generation system*, IEEE Transactions on Industrial Electronics, vol. 62, no. 9, pp. 5458-5467, Sept. 2015.

[22] A. Ahmad, et. al.: *Switched boost modified Z-source inverter topologies with improved voltage gain capability*, IEEE Journal of Emerging and Selected Topics in Power Electronics, Vol. 6, Issue 4, pp. 2227-2244, Dec. 2018.

[23] M. Nguyen and T. Tran: *A single-phase single-stage switched-boost inverter with four switches*, IEEE Transactions on Power Electronics, Vol. 33, Issue 8, pp. 6769-7681, Aug. 2018.

[24] P. Krause, et. al.: *Analysis of electric machinery and drive systems*, Third Edition, IEEE Press, 2013.

[25] V. Karthik, and S Kottayil,: *An improved PWM control of quasi-switched-boost inverter with reduced ripple magnitude and increased ripple frequency input current*, 2017 IEEE (TAP Energy) , India, pp. 1-6, 21-23 Dec., 2017.

[26] R. Adda, S. Mishra and A. Joshi,: *A PWM control strategy for switched boost inverter*, 2011 IEEE Energy Conversion Congress and Exposition, Phoenix, AZ, USA, pp. 991-996, 17-22 Sept. 2011.

[27] V. Anusree and P. Saifunnisa,: *Closed loop control of switched boost inverter*, IEEE 2016 (ICEEOT), India, pp. 3040-30443, 3-5 Mar 2016.

[28] S. Mishra, R. Adda, and A. Joshi,: *Inverse Watkins–Johnson topology-based inverter*, IEEE Transactions on Power Electronics, Vol. 27, Issue 3, pp. 1066-1070, March 2012.

[29] Y. Siwakoti, F. Blaabjerg and P. Loh,: *Z-source converters*, Book chapter of: *Power electronic converters and systems: frontiers and applications*, A. M. Trzynadlowski, Ed. Stevenage, U.K.: IET Press, pp. 205–243, Dec. 2015.

[30] L. Huang, M. Zhang, L. Hang, W. Yao, and Z. Lu,: *A family of three-switch three-state single-phase Z-source inverters*, IEEE Transactions on Power Electronics, Vol. 28, Issue 5, pp. 2317-2329, May 2013.

[31] Y. Liu, B. Ge, H. Abu-Rub, and F. Blaabjerg,: *Single-phase Z-source/ quasi-Z-source inverters and converters*, IEEE Industrial Electronics Magazine, Vol. 12, Issue 2, pp. 6-23, June 2018.

[32] W. Xu, et. al.,: *A series of new control methods for single-phase Z-source inverters and the optimized operation*, IEEE Access, Vol. 7, pp. 113786-113800, 2019.

[33] T Vijay Muni,: *Z-Source Inverter*, MATLAB Central File Exchange. Retrieved January 6, 2022.

[34] https://www.opal-rt.com/simulator-platform-op4510/

[35] https://www.opal-rt.com/resource center/document/?resource=L00161_0362